Subradiance with Saturated Atoms: Population Enhancement of the Long-Lived States

A. Cipris,[1] N. A. Moreira,[2] T. S. do Espirito Santo,[2] P. Weiss,[1] C. J. Villas-Boas,[3] R. Kaiser,[1] W. Guerin,[1] and R. Bachelard[3]

[1]*Université Côte d'Azur, CNRS, Institut de Physique de Nice, 06560 Valbonne, France*
[2]*Instituto de Física de São Carlos, Universidade de São Paulo, 13566-590 São Carlos, SP, Brazil*
[3]*Departamento de Física, Universidade Federal de São Carlos, Rodovia Washington Luís, km 235—SP-310, 13565-905 São Carlos, SP, Brazil*

(Received 16 September 2020; accepted 16 February 2021; published 12 March 2021)

Dipole-dipole interactions are at the origin of long-lived collective atomic states, often called subradiant, which are explored for their potential use in novel photonic devices or in quantum protocols. Here, we study subradiance beyond the single-excitation regime and experimentally demonstrate a 200-fold increase in the population of these modes, as the saturation parameter of the driving field is increased. We attribute this enhancement to a mechanism similar to optical pumping through the well-coupled superradiant states. The lifetimes are unaffected by the pump strength, as the system is ultimately driven toward the single-excitation sector. Our study is a new step in the exploration of the many-body dynamics of large open systems.

DOI: 10.1103/PhysRevLett.126.103604

Light is an excellent tool to encode and transmit information, yet it comes up short in terms of storage. It is then convenient to "write" the information into a material memory, before "reading" it out at a later time. Atoms and their artificial versions are natural candidates to fulfill that purpose, where photons are converted into atomic excitations. In this context, cold atoms benefit a substantial cross section to couple to light, and provide access to a broad range of lifetimes, with transition linewidths ranging from mHz to MHz, making them useful tools for quantum information processing [1] and quantum metrology [2], for instance.

Considering interactions between the atoms opens yet new possibilities to harness their potential. In particular, the dipole-dipole interaction, which rises precisely in the presence of photons, leads to a variety of collective responses [3,4], such as single-layer atomic mirrors [5], superradiance [6–9], and subradiance [10–13]. The two latter effects, which result from the dissipative coupling of multiple atoms to common electromagnetic modes, correspond to atomic modes of lifetimes orders of magnitude smaller or larger, respectively, than the single-atom one. The use of external fields has been proposed to transfer excitations between modes and thus realize write and read operations [14,15].

These subradiant states are, by essence, difficult to drive, due to their weak coupling to the external world. The protocols designed to address them have been tailored for the single-excitation regime [14–18], which represents a drop in the sea of the long-lived states originally predicted by Dicke [19].

In this work, we explore the many-excitation regime by increasing the pump strength and we report on a large increase of the excitations cast in the long-lived modes. This is interpreted as a process analogous to optical pumping (OP) [see Fig. 1(a)]: addressing the multiexcitation superradiant states, well coupled to the external drive, allows one to efficiently populate the long-lived states through decay processes. Using numerical simulations, the study of the dynamics of the many-excitation states reveals that the longest lifetimes are found in the modes with fewer excitations, toward which the system quickly decays.

The atomic cloud is modeled as an ensemble of N two-level emitters with positions $\mathbf{r}_j$, a transition frequency $\omega_a = kc = 2\pi c/\lambda$ between their ground and excited states g and e ($\sigma_m^- = |g_m\rangle\langle e_m|$ and $\sigma_m^+ = |e_m\rangle\langle g_m|$ the lowering and rising operators), and a transition linewidth Γ. The cloud is driven by a monochromatic field with Rabi frequency $\Omega(\mathbf{r})$, detuned from the transition by Δ. The dipole-dipole interaction relies on the coupling of the atomic dipoles through common radiation modes, which results in sub- and superradiant collective modes (see Ref. [20] and Refs. [21–25] for details on the model). In large dilute clouds, the strength of the cooperativity is captured by the on-resonance optical thickness $b_0 = \sigma_{\mathrm{sc}} \int \rho_a(0,0,z)dz$ rather than the density [6,7,11,26,27] (with the cloud center and the pump waist at the origin, $\mathbf{k}_{\mathrm{laser}} = k\hat{z}$, and σ_{sc} the atom cross section).

Although our main focus is many-atom subradiance, let us first discuss the case of a pair of close atoms ($r_{12} \ll \lambda$) as a toy model, since it already captures the main features of our scheme. We consider a pump whose propagation axis is aligned with the two atoms [$\Omega(\mathbf{r}) = \Omega_0 e^{ikz}$ and $\mathbf{r}_2 - \mathbf{r}_1 = r_{12}\hat{z}$]. In the scalar light approximation, the dipole-dipole interaction generates two collective single-

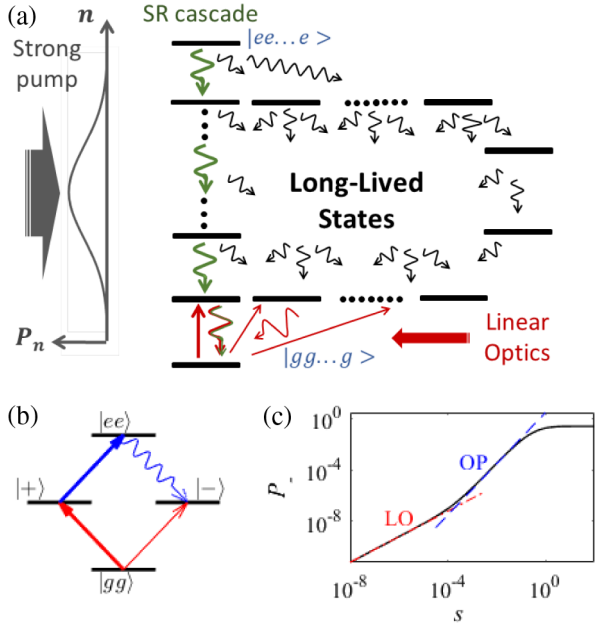

FIG. 1. (a) Dicke space for $N \gg 1$ two-level atoms, where the downward arrows depict the decay processes. The processes in green refer to the Dicke superradiant cascade through symmetric states [19], and the red ones to the linear-optics (LO) processes (i.e., the single-excitation regime). P_n schematically shows the population of the n-excitation states for a strong pump, illustrating the spread over various excitation numbers. (b) Energy levels for $N = 2$ coupled atoms (see main text for details). (c) Computed population of the long-lived $|-\rangle$ state for $N = 2$ coupled atoms. The red dash-dotted curve corresponds to $P_- = s_-/2 \propto s$, while the dashed blue one scales as s^2 (labeled OP). Simulation realized for $N = 2$ atoms distant of $kr = 0.05$, aligned with the pump axis, with a detuning $\Delta = -500\Gamma$.

excitation eigenstates $|\pm\rangle = (|eg\rangle \pm |ge\rangle)/\sqrt{2}$, in addition to the ground $|gg\rangle$ and double-excited $|ee\rangle$ states [see Fig. 1(b)]. These two collective states present decay rates $\Gamma_\pm = \Gamma \pm \Gamma_{12} = \Gamma[1 \pm \sin(kr_{12})/(kr_{12})]$ and energy shifts $\Delta_\pm = \pm\cos(kr_{12})/2kr_{12}$. The increased (reduced) lifetimes corresponding to Γ_- (Γ_+) can be interpreted as stemming from constructive (destructive) interference of the emission from the atoms [28,29]. The energy shifts are here neglected since we consider a pump with frequency far from the resonance of any mode ($|\Delta| \gg \Gamma, |\Delta_\pm|$), to avoid specific effects such as blockade [30,31] or antiblockade [32] of excitations. Importantly, the pump couples mostly to the superradiant $|+\rangle$ state, and very weakly to the long-lived $|-\rangle$ one, and we introduce the effective Rabi frequency for each mode: $\Omega_+ = \sqrt{2}\cos(kr_{12}/2)\Omega_0$ and $\Omega_- = \sqrt{2}\sin(kr_{12}/2)\Omega_0$ (up to a phase), which can be identified by rewriting the driving Hamiltonian in terms of the states $|+\rangle$ and $|-\rangle$.

The steady-state population of the long-lived mode then presents three typical regimes, depending on the pump strength. First, for the lowest intensities (linear-optics regime), the population of $|ee\rangle$ is negligible and the single-excitation modes $|\pm\rangle$ are driven only directly from the pump, so one obtains the following scaling for their population: $P_\pm \approx s_\pm/2 \propto s$, with $s_\pm = 2\Omega_\pm^2/[\Gamma_\pm^2 + 4(\Delta \mp \Delta_{12}/2)^2]$ the effective saturation parameter for each mode, and $s = 2\Omega_0^2/(\Gamma^2 + 4\Delta^2)$ the single-atom one [see Fig. 1(c)]. This single-excitation regime holds for $s_\pm \ll 1$, i.e., $\Omega_+ \ll \Delta$.

As the drive strength is increased, the doubly-excited state $|ee\rangle$ is substantially populated thanks to the strong coupling of the drive to the superradiant state: $P_+ \approx s_+/2 \propto s$ and $P_{ee} \propto s^2$. Then, the $|-\rangle$ states get an additional population by decay from $|ee\rangle$, at rate Γ_-, leading to a long-lived population that grows quadratically with the saturation parameter: $P_- \propto s^2$ [see Fig. 1(c)].

Finally, for the largest values of the saturation parameter, i.e., with a Rabi frequency such that the dynamics of each atom is dominated by the drive ($\Omega_0 \gg \Delta \gg \Gamma, |\Delta_\pm|$), the system is cast into a separable state described by the density matrix $\hat{\rho} = \otimes_{j=1,2}\,(|g_j\rangle\langle g_j| + |e_j\rangle\langle e_j|)/2$. This mixed state projects equally on the states $|gg\rangle$, $|+\rangle$, $|-\rangle$, and $|ee\rangle$, resulting in $P_- \approx 1/4$. Hence, the strong pump overcomes the weak coupling of subradiant modes which, in the linear-optics regime, prevents one to populate them efficiently. The present mechanism is analogous to optical pumping, where an excited state (here $|ee\rangle$) is directly driven by the laser, and induces a population in the long-lived state (here $|-\rangle$) by incoherent decay.

Despite its extreme simplicity, let us now discuss how the $N = 2$ case captures the essential features of our many-atom experiment, based on a cold atomic cloud of $N \approx 6 \times 10^9$ randomly distributed ^{87}Rb atoms prepared in a magneto-optical trap. A detailed description of the setup and of the methods for observing subradiance can be found in Refs. [11,33,34]. In this new series of experiment, an extra care has been taken to control the possible detrimental effects of the large intensity probe on the atomic cloud: we reduced the pulse duration to 5 μs and added a repumper pulse between each probe pulse. Moreover, we used an improved characterization of the sample, as described in Refs. [20,34]. We varied the saturation parameter in the range $3 \times 10^{-3} \lessapprox s(\Delta) \lessapprox 2$ by varying the intensity of the probe beam [20].

To obtain the amplitude A_- and the lifetime τ_- of the long-lived radiation we fit the collected intensity by an exponential $I(t) = A_- \exp(-t/\tau_-)$ in a range $t \in [150; 250]/\Gamma$ (see Supplemental Material [20] for a few decay curves). The normalized population $P_- \propto A_-\tau_-/N$ of these long-lived states, defined as the number of excitations divided by the atom number, can be deduced by assuming that the long-lived excitations are radiated isotropically, and taking into account the collection efficiency of the detection. The measured population is presented in Fig. 2(a) for a fixed $b_0 = 54$. It undergoes a 200-fold increase, from 3×10^{-7} to 7×10^{-5}, as the saturation parameter is increased from $s \approx 3 \times 10^{-3}$ to 0.3.

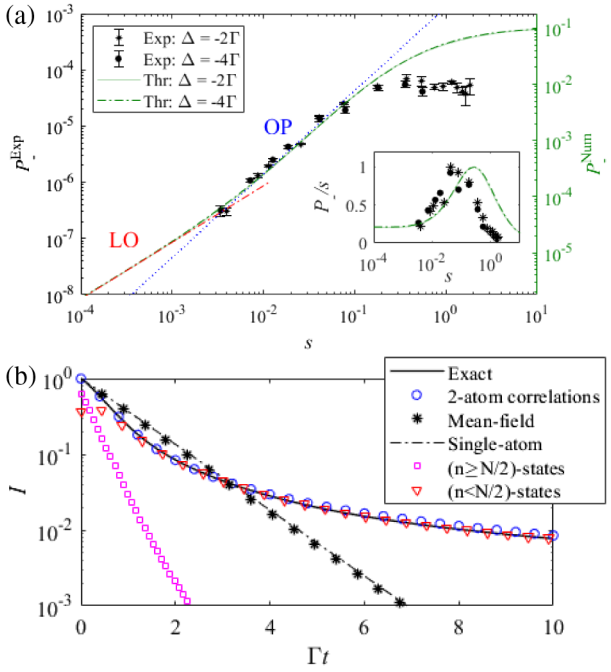

FIG. 2. (a) Normalized population P_- of long-lived states as a function of the saturation parameter. Experimental data (symbols, left axis) acquired for $b_0 = 54 \pm 2$, with error bars describing the 95% confidence bounds (statistical uncertainty only). Simulations (lines, right axis) realized for $b_0 \approx 5$ and $N = 100$, averaging over 40 realizations (error bars of order 1%, not shown here). The blue (red) dotted line stands for a fit $P \propto s^\beta$, with $\beta = 1.49 \pm 0.23$ (1.007 ± 0.010). Inset: Ratio population over saturation parameter P_-/s, with a maximum normalized to unity. (b) Dynamics of the radiated intensity after switching-off the pump at $t = 0$, for $N = 7$ atoms, $b_0 = 5$ (using 60 realizations), $\Delta = -2\Gamma$ and $s = 50$. Simulations realized using exact simulations (plain curve), the pair-correlation approach (circles) and the mean-field model (stars). The contribution from states with $n \geq 4$ (squares) and $n \leq 3$ (triangles) are computed separately, for the exact simulations.

This corresponds to a maximum number of $\approx 4 \times 10^5$ excitations in these long-lived modes. Note that these numbers are only orders of magnitude since the detection efficiency (solid angle, quantum efficiency of the detector, various losses on the optical path) is not precisely calibrated. More importantly, we observe a superlinear scaling of the population, $P_- \propto s^\beta$ with $\beta = 1.49 \pm 0.23$ in the experimental data (using a 95% confidence interval), to be compared to the linear scaling $\beta = 1.007 \pm 0.010$ (from the simulations). This is illustrated in the inset of Fig. 2, where P_-/s is plotted. This scaling has been observed for several values of b_0 [20].

Furthermore, subradiant modes with different lifetimes can be harnessed by considering different time windows of the decay dynamics. We have checked that the population of modes with lifetimes ~ 40–$100\Gamma^{-1}$ also exhibit a superlinear growth as $\sim s^{1.5}$, and a maximum value of $\approx 10^{-4}$ [20]. This suggests that although longer-lived modes are expected to be much less populated in a linear-optics scenario (because of the weaker coupling to the external world), the much larger connectivity between the modes introduced by the strong pump and the decay channels enhances their population.

This superlinear growth of the long-lived population is a clear indication of beyond-linear-optics pumping of these modes and calls for a more specific study. Yet such a study requires addressing its size-2^N Hilbert space, which unavoidably leads to drastic approximations. First, we note that the lifetime of collective modes in these clouds has been shown to scale with the cooperativity parameter b_0 [6,7,11,27], which scales as $N/(kR)^2$ (with R the cloud radius). Spherical Gaussian clouds are used in all simulations, as in the experiment. This allows one to compare the collective effects in the experiment and in simulations despite the very different atom numbers, by tuning the cloud radius.

Second, simulating the dynamics of more than a dozen saturated two-level atoms requires additional approximations in describing the system state. We here resort to a truncated scheme based on the Bogoliubov-Born-Green-Kirkwood-Yvon approach, where the density matrix is recast as a sum of reduced density matrices of order $m = 1\ldots, N$, thus establishing a hierarchy of quantum correlations [35]. The truncation of the hierarchy to two-particle quantum correlations has proven to be an efficient technique to simulate the dynamics of strongly driven atomic clouds [36,37], and we refer to these references for further details.

We have benchmarked the truncated method by comparing the late-time, far-field radiated intensity $I_{\mathbf{k}} \propto \sum_{m,n} e^{i\mathbf{k}.(\mathbf{r}_m - \mathbf{r}_n)} \langle \hat{\sigma}_m^+ \hat{\sigma}_n^- \rangle$ to that from exact simulations 38,39]] [see example in Fig. 2(b)], obtaining accurate results for atomic densities up to $\rho_a \approx 0.03k^3$ (for random distributions with a minimal distance $\rho_a^{-1/3}/2$). Interestingly, we observe that semiclassical simulations (i.e., a truncation at the first order) fail to capture the long-lived states, as they exhibit a single-atom decay dynamics for a strong drive [see Fig. 2(b)]. This is in contrast with the superradiant cascade, known to be described by a semiclassical approach [19,40–43], and it strongly suggests that the subradiant states here studied might be a source of quantum correlations [44].

The normalized population obtained from simulations with the truncated scheme are presented as continuous and dashed lines in Fig. 2(a), and present a good agreement with the experimental data. The absence of dependence on the detuning validates the earlier hypothesis of negligible frequency shifts. Although there is some discrepancy in the values of the normalized population (which might be due to the vastly different parameters for the atom number and size of the sample), the scaling $P_- \propto s^{1.49}$ observed in the experiment is well consistent with the one observed in both truncated and exact simulations [20].

Interestingly, it also shows that even with a saturation parameter as low as $s \approx 3 \times 10^{-3}$, the linear-optics regime describing the single-excitation physics is not reached, in the presence of cooperative effects. The simulations at $b_0 = 5$ present a nonlinearity threshold at $s_{\mathrm{LO}} \approx 2 \times 10^{-3}$, yet it was not possible to obtain a scaling of s_{LO} from the low-b_0 simulations. Nevertheless, we note that the $N = 2$ case discussed earlier suggests that longer-lived states (achieved for smaller distances kr) couple less to the pump, which in turn results in lower values of s_{LO} [$s_{\mathrm{LO}} \sim 10^{-4}$ in Fig. 1(c)]. Furthermore, it was recently suggested that such a threshold may scale as $\Gamma_n^{2.5}$, with Γ_n the nth mode linewidth [45]: Assuming the subradiant states present linewidths scaling as $\Gamma_n \sim \Gamma/b_0$ [11], saturation parameters orders of magnitude smaller may be necessary to experimentally reach the linear-optics regime for long-lived states.

Increasing the pump power opens the possibility of exploring a much broader part of the 2^N-dimensional Hilbert space, and thus potentially access much longer lifetimes—the $N = 2$ case only yields one superradiant and one long-lived state. Nonetheless, as observed in Fig. 3(a), the lifetime of the long-lived modes is only marginally affected by the strength of the drive. While the simulations of the truncated dynamics present an increase of ∼15% in lifetime as the saturation parameter is increased, the experimental error bars do not permit us to identify this increase.

To understand better the preservation of the long lifetimes, studying all the collective modes of the system is not relevant since the question is rather about which ones are populated by the pump [46]. Thus, we monitor the decay dynamics of the population of the n-excitation states, $P_n = \mathrm{Tr}(\hat{P}_n \hat{\rho})$, where we have introduced the projector $\hat{P}_n = \sum_{\mathcal{P}} \bigotimes_{j=1}^{n} |e_j\rangle\langle e_j| \bigotimes_{m=n+1}^{N} |g_m\rangle\langle g_m|$, with $\mathcal{P}$ the $N!/n!(N-n)!$ permutations of a set with n excited atoms and $(N-n)$ in the ground state.

The evolution of the population of n-excitation states is presented in Fig. 3(c), where we observe that, after a short transient of order $1/\Gamma$, the lower the excitation number n, the slower the decay: Highly excited states decay quickly into low-excitation ones, where the excitations remain for long times, as compared to $1/\Gamma$. A systematic analysis of the dynamics, for atom numbers ranging from 4 to 9, reveals that states from the upper part of the Dicke space ($n > N/2$) decay at superradiant rates (even at late times), whereas the lower part ($n \leq N/2$) is characterized by long lifetimes (at late times), see Fig. 3(d). Consequently, the short-time (superradiant) emission is realized by highly excited states, whereas the late-time emission comes from low-excitation ones. This is illustrated in Fig. 2(b), where the contribution to the radiated intensity of low- and high-excitation states were computed separately. Another consequence is that an increased pump strength populates subradiant states with shorter lifetimes, so the radiation from low-excitation, longer-lived, states may dominate later, see the Supplemental Material [20]. Finally, we have checked that starting from a fully inverted system, as originally studied by Dicke [19], the initial (superradiant) dynamics differs from that of a cloud driven to steady state with a strong pump, yet the same long lifetimes are eventually observed (not shown here): The superradiant cascade occurs, yet not without some decay toward longer-lived modes, as illustrated in Fig. 1(a).

Hence, the $n \geq 2$ part of the Hilbert space, which comprises everything beyond linear optics, does not appear to offer access to longer lifetimes, nor does it provide a path to escape long-lived modes. Remarkably, a study on one-

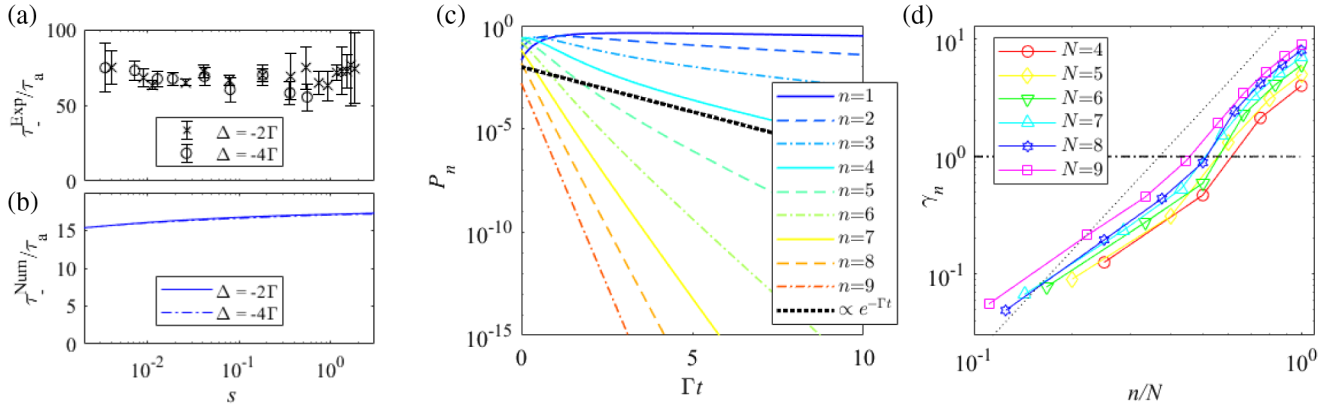

FIG. 3. (a)–(b) Lifetime of the long-lived modes as a function of the saturation parameter, from (a) the experimental data and (b) the simulations of the truncated dynamics [same parameters and same conventions for the error bars as in Fig. 2(a)]. (c) Dynamics of the population P_n of the n-excitation states for a cloud of $N = 9$ atoms ($\rho_a = 0.3k^3$), initially driven to steady state by a strong resonant field with $\Omega_0 = 5\Gamma$ (the ground state one, $P_0 = 1 - \sum_{n\geq 1}$, is not shown here). (d) Decay rate γ_n of the populations P_n, computed for $t \in [5; 10]/\Gamma$, as a function of the relative excitation number n/N, and for particle numbers from $N = 4$ to 9 ($\rho_a = 0.3k^3$, $\Omega_0 = 5\Gamma$). The horizontal line marks the $\gamma_n = 1$ transition from subradiant to superradiant states, while the dotted black line, which scales as n^3, is only a guide for the eye.

dimensional regular chains has reached the similar conclusion that the *longest-lived* higher-excitation states present a decay rate that scales as $(n/N)^3$ [24], in excellent agreement with our simulations [see the dotted line in Fig. 3(d)]. This suggests that this feature may be quite universal, beyond the details of geometry and dimensionality of the system.

In conclusion, we have reported on the experimental observation that long-lived subradiant states can have their population enhanced by increasing the pump strength, through a mechanism similar to optical pumping via superradiant states. Surprisingly, the single-excitation (linear-optics) subspace actually presents the longest lifetimes. Note that despite multiple theoretical papers and several experimental results, a comprehensive understanding including an analytical description of subradiance is still lacking, even in the weak driving limit, let alone for strong driving.

In particular, the faster decay of higher-excitation states leads to the puzzling question of the entanglement of these long-lived states created through decay processes [44], as the difference between a true single-excitation state [47,48] and its linear-optics separable counterpart resides in the multi-excitation component [49,50]. The failure of a semiclassical approach to describe properly those decay processes is a further argument to support the idea that the subradiant states might be appropriate to store entanglement or quantum correlations. Finally, the present scheme could, in principle, be applied to cavity setups, where the light from subradiant states could be collected more efficiently in the cavity modes, for example, using external fields [15].

Part of this work was performed in the framework of the European Training Network ColOpt, which is funded by the European Union (EU) Horizon 2020 program under the Marie Sklodowska-Curie action, Grant Agreement No. 721465, and the project ANDLICA, ERC Advanced Grant No. 832219. We also acknowledge funding from the French National Research Agency (projects PACE-IN ANR19-QUAN-003 and QuaCor ANR19-CE47-0014). R. B., T. S. E. S., and C. J. V.-B. benefited from Grants from São Paulo Research Foundation (FAPESP, Grants No. 2018/01447-2, No. 2018/15554-5, No. 2018/12653-2, No. 2019/13143-0, No. 2019/02071-9, and No. 2019/11999-5) and from the National Council for Scientific and Technological Development (CNPq, Grants No. 302981/2017-9, No. 409946/2018-4, and No. 307077/2018-7). R. B. and R. K. received support from the project CAPES-COFECUB (Ph879-17/CAPES 88887.130197/2017-01). P. W. received support from the Deutsche Forschungsgemeinschaft (Grant No. WE 6356/1-1).

[1] K. Hammerer, A. S. Sørensen, and E. S. Polzik, Quantum interface between light and atomic ensembles, Rev. Mod. Phys. **82**, 1041 (2010).

[2] L. Pezzè, A. Smerzi, M. K. Oberthaler, R. Schmied, and P. Treutlein, Quantum metrology with nonclassical states of atomic ensembles, Rev. Mod. Phys. **90**, 035005 (2018).

[3] D. V. Kupriyanov, I. M. Sokolov, and M. D. Havey, Mesoscopic coherence in light scattering from cold, optically dense and disordered atomic systems, Phys. Rep. **671**, 1 (2017).

[4] W. Guerin, M. T. Rouabah, and R. Kaiser, Light interacting with atomic ensembles: Collective, cooperative and mesoscopic effects, J. Mod. Opt. **64**, 895 (2017).

[5] J. Rui, D. Wei, A. Rubio-Abadal, S. Hollerith, J. Zeiher, D. M. Stamper-Kurn, C. Gross, and I. Bloch, A subradiant optical mirror formed by a single structured atomic layer, Nature **583**, 369 (2020).

[6] M. O. Araújo, I. Krešić, R. Kaiser, and W. Guerin, Superradiance in a Large and Dilute Cloud of Cold Atoms in the Linear-Optics Regime, Phys. Rev. Lett. **117**, 073002 (2016).

[7] S. J. Roof, K. J. Kemp, M. D. Havey, and I. M. Sokolov, Observation of Single-Photon Superradiance and the Cooperative Lamb Shift in an Extended Sample of Cold Atoms, Phys. Rev. Lett. **117**, 073003 (2016).

[8] L. Ortiz-Gutiérrez, L. F. Muñoz Martínez, D. F. Barros, J. E. O. Morales, R. S. N. Moreira, N. D. Alves, A. F. G. Tieco, P. L. Saldanha, and D. Felinto, Experimental Fock-State Superradiance, Phys. Rev. Lett. **120**, 083603 (2018).

[9] S. Okaba, D. Yu, L. Vincetti, F. Benabid, and H. Katori, Superradiance from lattice-confined atoms inside hollow core fibre, Commun. Phys. **2**, 136 (2019).

[10] T. Bienaimé, N. Piovella, and R. Kaiser, Controlled Dicke Subradiance from a Large Cloud of Two-Level Systems, Phys. Rev. Lett. **108**, 123602 (2012).

[11] W. Guerin, M. O. Araújo, and R. Kaiser, Subradiance in a Large Cloud of Cold Atoms, Phys. Rev. Lett. **116**, 083601 (2016).

[12] P. Solano, P. Barberis-Blostein, F. K. Fatemi, L. A. Orozco, and S. L. Rolston, Super-radiance reveals infinite-range dipole interactions through a nanofiber, Nat. Commun. **8**, 1857 (2017).

[13] D. Das, B. Lemberger, and D. D. Yavuz, Subradiance and superradiance-to-subradiance transition in dilute atomic clouds, Phys. Rev. A **102**, 043708 (2020).

[14] M. O. Scully, Single photon subradiance: Quantum Control of Spontaneous Emission and Ultrafast Readout, Phys. Rev. Lett. **115**, 243602 (2015).

[15] G. Facchinetti, S. D. Jenkins, and J. Ruostekoski, Storing Light with Subradiant Correlations in Arrays of Atoms, Phys. Rev. Lett. **117**, 243601 (2016).

[16] A. Kalachev and S. Kröll, Coherent control of collective spontaneous emission in an extended atomic ensemble and quantum storage, Phys. Rev. A **74**, 023814 (2006).

[17] A. Kalachev, Quantum storage on subradiant states in an extended atomic ensemble, Phys. Rev. A **76**, 043812 (2007).

[18] Y. He, L. Ji, Y. Wang, L. Qiu, J. Zhao, Y. Ma, X. Huang, S. Wu, and D. E. Chang, Geometric Control of Collective Spontaneous Emission, Phys. Rev. Lett. **125**, 213602 (2020).

[19] R. H. Dicke, Coherence in spontaneous radiation processes, Phys. Rev. **93**, 99 (1954).

[20] See Supplemental Material at http://link.aps.org/supplemental/10.1103/PhysRevLett.126.103604 for the

calibration of the saturation parameter, the characterization of the atomic sample including the effects of the probe pulses, a few illustrative subradiant decay curves, the superlinear behavior of the long-lived mode population for different values of b_0, and the population of subradiant modes of different lifetimes.

[21] M. J. Stephen, First-order dispersion forces, J. Chem. Phys. **40**, 669 (1964).

[22] R. H. Lehmberg, Radiation from an N-atom system. I. General formalism, Phys. Rev. A **2**, 883 (1970).

[23] R. Friedberg, S. R. Hartmann, and J. T. Manassah, Frequency shifts in emission and absorption by resonant systems ot two-level atoms, Phys. Rep. C **7**, 101 (1973).

[24] A. Asenjo-Garcia, M. Moreno-Cardoner, A. Albrecht, H. J. Kimble, and D. E. Chang, Exponential Improvement in Photon Storage Fidelities Using Subradiance and "Selective Radiance" in Atomic Arrays, Phys. Rev. X **7**, 031024 (2017).

[25] T. S. do Espirito Santo, P. Weiss, A. Cipris, R. Kaiser, W. Guerin, R. Bachelard, and J. Schachenmayer, Collective excitation dynamics of a cold atom cloud, Phys. Rev. A **101**, 013617 (2020).

[26] W. Guerin, T. S. do Espirito Santo, P. Weiss, A. Cipris, J. Schachenmayer, R. Kaiser, and R. Bachelard, Collective Multimode Vacuum Rabi Splitting, Phys. Rev. Lett. **123**, 243401 (2019).

[27] A. Cipris, R. Bachelard, R. Kaiser, and W. Guerin, Van der waals dephasing for dicke subradiance in cold atomic clouds, arXiv:2012.06248.

[28] E. A. Power, Effect on the lifetime of an atom undergoing a dipole transition due to the presence of a resonating atom, J. Chem. Phys. **46**, 4297 (1967).

[29] A. A. Svidzinsky, J. T. Chang, and M. O. Scully, Cooperative spontaneous emission of n atoms: Many-body eigenstates, the effect of virtual lamb shift processes, and analogy with radiation of n classical oscillators, Phys. Rev. A **81**, 053821 (2010).

[30] A. Cidrim, T. S. do Espirito Santo, J. Schachenmayer, R. Kaiser, and R. Bachelard, Photon Blockade with Ground-State Neutral Atoms, Phys. Rev. Lett. **125**, 073601 (2020).

[31] L. A. Williamson, M. O. Borgh, and J. Ruostekoski, Superatom Picture of Collective Nonclassical Light Emission and Dipole Blockade in Atom Arrays, Phys. Rev. Lett. **125**, 073602 (2020).

[32] K. Almutairi, R. Tanaś, and Z. Ficek, Generating two-photon entangled states in a driven two-atom system, Phys. Rev. A **84**, 013831 (2011).

[33] P. Weiss, M. O Araújo, R. Kaiser, and W. Guerin, Subradiance and radiation trapping in cold atoms, New J. Phys. **20**, 063024 (2018).

[34] P. Weiss, A. Cipris, M. O. Araújo, R. Kaiser, and W. Guerin, Robustness of Dicke subradiance against thermal decoherence, Phys. Rev. A **100**, 033833 (2019).

[35] M. Bonitz, *Quantum Kinetic Theory* (Springer International Publishing, Cham, 2016).

[36] S. Krämer and H. Ritsch, Generalized mean-field approach to simulate the dynamics of large open spin ensembles with long range interactions, Eur. Phys. J. D **69**, 282 (2015).

[37] L. Pucci, A. Roy, T. S. do Espirito Santo, R. Kaiser, M. Kastner, and R. Bachelard, Quantum effects in the cooperative scattering of light by atomic clouds, Phys. Rev. A **95**, 053625 (2017).

[38] J. R. Johansson, P. D. Nation, and F. Nori, QuTiP: An open-source PYTHON framework for the dynamics of open quantum systems, Comput. Phys. Commun. **183**, 1760 (2012).

[39] J. R. Johansson, P. D. Nation, and F. Nori, QuTiP2: A PYTHON framework for the dynamics of open quantum systems, Comput. Phys. Commun. **184**, 1234 (2013).

[40] F. T. Arecchi, E. Courtens, R. Gilmore, and H. Thomas, Atomic coherent states in quantum optics, Phys. Rev. A **6**, 2211 (1972).

[41] J. C. MacGillivray and M. S. Feld, Theory of superradiance in an extended, optically thick medium, Phys. Rev. A **14**, 1169 (1976).

[42] M. Gross and S. Haroche, Superradiance: An essay on the theory of collective spontaneous emission, Phys. Rep. **93**, 301 (1982).

[43] C. E. Máximo, R. Bachelard, F. E. A. dos Santos, and C. J. Villas-Boas, Cooperative spontaneous emission via a renormalization approach: Classical versus semiclassical effects, Phys. Rev. A **101**, 023829 (2020).

[44] R. Tana and Z. Ficek, Entangling two atoms via spontaneous emission, J. Opt. B **6**, S90 (2004).

[45] L. A. Williamson and J. Ruostekoski, Optical response of atom chains beyond the limit of low light intensity: The validity of the linear classical oscillator model, Phys. Rev. Research **2**, 023273 (2020).

[46] W. Guerin and R. Kaiser, Population of collective modes in light scattering by many atoms, Phys. Rev. A **95**, 053865 (2017).

[47] M. O. Scully, E. S. Fry, C. H. Raymond Ooi, and K. Wódkiewicz, Directed Spontaneous Emission from an Extended Ensemble of N Atoms: Timing is Everything, Phys. Rev. Lett. **96**, 010501 (2006).

[48] F. Fröwis, P. C. Strassmann, A. Tiranov, C. Gut, J. Lavoie, N. Brunner, F. Bussières, M. Afzelius, and N. Gisin, Experimental certification of millions of genuinely entangled atoms in a solid, Nat. Commun. **8**, 907 (2017), .

[49] J. H. Eberly, Emission of one photon in an electric dipole transition of one among N atoms, J. Phys. B **39**, S599 (2006).

[50] T. Bienaimé, M. Petruzzo, D. Bigerni, N. Piovella, and R. Kaiser, Atom and photon measurement in cooperative scattering by cold atoms, J. Mod. Opt. **58**, 1942 (2011).

Subradiance with saturated atoms: population enhancement of the long-lived states: Supplemental material

A. Cipris,[1] N. A. Moreira,[2] T. S. do Espirito Santo,[2] P. Weiss,[1]
C. J. Villas-Boas,[3] R. Kaiser,[1] W. Guerin,[1] and R. Bachelard[3]

[1] *Université Côte d'Azur, CNRS, Institut de Physique de Nice, France*
[2] *Instituto de Física de São Carlos, Universidade de São Paulo - 13560-970 São Carlos, SP, Brazil*
[3] *Departamento de Física, Universidade Federal de São Carlos, Rod. Washington Luís, km 235 - SP-310, 13565-905 São Carlos, SP, Brazil*

I. COUPLED DIPOLE MODEL FOR N TWO-LEVEL ATOMS IN FREE SPACE

The atomic cloud is modelled as an ensemble of N two-level emitters with positions $\mathbf{r}_j$ and rising/lowering operators $\hat{\sigma}_j^+/\hat{\sigma}_j^-$ between their ground and excited states g and e; $\omega_a = kc = 2\pi c/\lambda$ is the transition frequency and Γ its linewidth. The cloud is driven by a near-resonance monochromatic field with Rabi frequency $\Omega(\mathbf{r})$, detuned from the transition by Δ. Within the Markov and rotating-wave approximations, the coupled dynamics of the evolution of the density matrix $\hat{\rho}$ describing the atomic dipoles is obtained from the master equation $\dot{\hat{\rho}} = -i[H,\hat{\rho}] + \mathcal{L}(\hat{\rho})$, where the coherent Hamiltonian $\hat{H}$ and dissipative dynamics $\mathcal{L}$ are given, in the pump frame, by [1–3]:

$$\hat{H} = -\Delta \sum_m \hat{\sigma}_m^+ \hat{\sigma}_m^- + \frac{1}{2}\sum_m \left[\Omega(\mathbf{r}_m)\hat{\sigma}_m^+ + h.c.\right] + \frac{1}{2}\sum_{m,n\neq m} \Delta_{mn}\hat{\sigma}_m^+\hat{\sigma}_n^-, \tag{1a}$$

$$\mathcal{L}(\hat{\rho}) = \frac{1}{2}\sum_{m,n}\Gamma_{nm}\left(2\hat{\sigma}_m^-\hat{\rho}\hat{\sigma}_n^+ - \hat{\sigma}_n^+\hat{\sigma}_m^-\hat{\rho} - \hat{\rho}\hat{\sigma}_n^+\hat{\sigma}_m^-\right). \tag{1b}$$

The diagonal term corresponds to the single-atom dynamics, $\Gamma_{nn} = \Gamma = 1$ and $\Delta_{nn} = 0$, while the coupling terms are given by $\Delta_{mn} = -\Gamma\cos(kr_{mn})/(kr_{mn})$ and $\Gamma_{mn} = \Gamma\sin(kr_{mn})/(kr_{mn})$, with $r_{mn} = |\mathbf{r}_m - \mathbf{r}_n|$. This model corresponds to a 'scalar light' approximation: although polarization can play an important role in sub-wavelength clouds [4, 5], the experimental situation is that of a dilute cloud (atomic density $\rho_a \approx 0.06\lambda^{-3}$), where a scalar description of the light is a good approximation [6].

II. CALIBRATION OF THE SATURATION PARAMETER

In this experiment, it is important to have a proper calibration of the saturation parameter, defined as

$$s(\delta) = g\frac{s_0}{1+4(\Delta/\Gamma)^2}, \tag{2}$$

where $g = 7/15$ is the degeneracy factor of the $|F=2\rangle \to |F'=3\rangle$ D_2 transition of ^{87}Rb for a statistical mixture of equally populated Zeeman sublevels and $s_0 = I/I_{\rm sat}$ is the on-resonance saturation parameter, with $I_{\rm sat} = 1.6\,\mathrm{mW/cm^2}$ the saturation intensity. A first evaluation of the saturation parameter at the center of the beam can be obtained from the measurement of the beam power and its waist ($1/e^2$ radius $w = 5.3$ mm), but this is usually not precise because of a number of effects: losses along the beam path, beam not perfectly Gaussian, atomic cloud not perfectly at the center of the beam, etc. A calibration method based on the interaction with the atoms is thus preferable. Hereafter we use the label $s'(\Delta)$ for the saturation parameter that is determined by measuring the power and waist of the probe beam, while for the properly calibrated saturation parameter we use $s(\Delta)$. Note that the probe power is measured simultaneously to the data acquisition by a dedicated detector.

The first calibration method is based on the measurement of the fluorescence level. The atomic cloud ($b_0 = 37 \pm 1$) was illuminated by the probe beam with $\Delta = -4\Gamma$ and the fluorescence signal was recorded as a function of $s'(\Delta)$ [Fig. S1(a)]. Since the total scattering rate is $\propto s/(s+1)$, we fitted the measured fluorescence level by $f = Bs'/(Cs'+1)$ and we obtained a correction factor for the saturation parameter $C = 0.36 \pm 0.04$.

The other two calibration methods rely on hyperfine depumping into the $|F=1\rangle$ ground state. Although the transition of interest in this experiment is $|F=2\rangle \to |F'=3\rangle$, when the probe beam is largely detuned to the red from that transition, there is a significant probability of exciting the $|F'=2\rangle$ state, from which atoms can decay into the dark $|F=1\rangle$ state. The corresponding depumping rate is given by

$$\Gamma_{\rm depump} = p_{21}\frac{\Gamma}{2}\frac{s_{22}}{s_{22}+1},\ \text{with}\ s_{22} = g_{22}\frac{s_0}{1+4(\Delta_{22}/\Gamma)^2},$$

where $p_{21} = 1/2$ is the decay probability of $|F'=2\rangle$ towards $|F=1\rangle$, s_{22} is the saturation parameter for the $|F=2\rangle \to |F'=2\rangle$ transition, with $g_{22} = 1/6$ the corresponding degeneracy factor, and $\Delta_{22} = 44\Gamma + \Delta$ the corresponding detuning. By measuring the number of atoms in the $|F=2\rangle$ as a function of time, $N(t) = N_0\exp(-\Gamma_{\rm depump}t)$, we can extract the depumping rate and then the saturation parameter.

At sufficiently large detuning, the fluorescence level is proportional to the number of atoms, so the depumping rate can be obtained by measuring the fluorescence level as a function of the laser duration. In fact, since

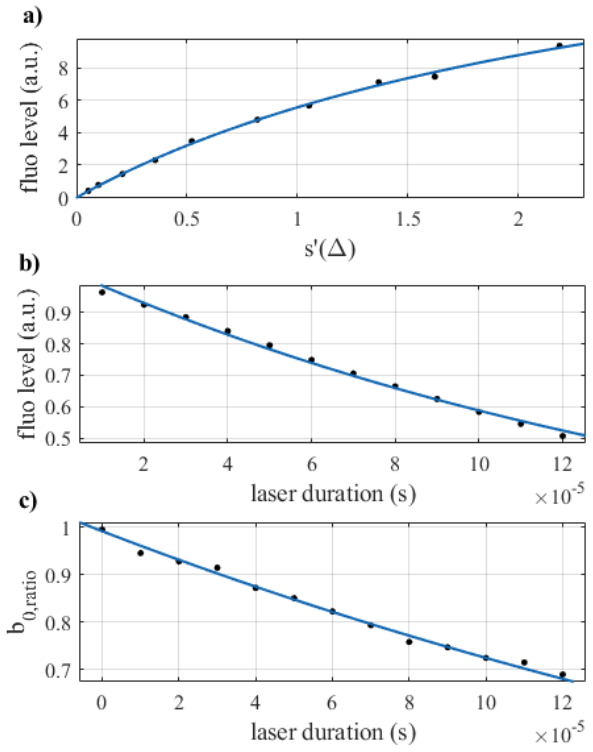

Fig. S 1. Different calibration methods of the saturation parameter. Black dots represent experimental data, while blue solid lines are fit curves. a) Measured fluorescence level as a function of the roughly-determined saturation parameter $s'(\Delta)$, together with the fit function $f = Bs'/(Cs' + 1)$. Experimental data was obtained with $b_0 = 37 \pm 1$, $\Delta = -4\Gamma$ and a pulse duration of $5\,\mu$s. b) Measured fluorescence level as a function of the total interaction time with the probe beam, fitted by an exponential decay corresponding to the depumping rate $\Gamma_{\text{depump}} = (1.51 \pm 0.07) \times 10^{-4}\Gamma$. The measurement was done with $\Delta = -10\Gamma$ and a pulse duration of $10\,\mu$s. c) Ratio between measured b_0 without and with repumping as a function of the total interaction time with the probe beam. The exponential fit to the experimental data gave $\Gamma_{\text{depump}} = (8.37 \pm 0.03) \times 10^{-5}\Gamma$. The data were obtained with $\Delta = -8\Gamma$ and a pulse duration of $10\,\mu$s.

we illuminated the atomic cloud by series of 12 pulses of duration $10\,\mu$s each, we added up the duration of subsequent pulses. By fitting an exponential decay to the measured fluorescence level [Fig. S1(b)], we obtained the depumping rate, from which we determined the saturation parameter. This method yielded the correction factor $C = 0.32 \pm 0.01$.

Another way of obtaining the depumping rate is by measuring the optical thickness as a function of the laser duration with and without a repumping stage just before absorption imaging. Then, by fitting the ratio by an exponential decay [Fig. S1(c)], we extracted the depumping rate and with that we obtained the correction factor $C = 0.34 \pm 0.01$.

The three methods are in very good agreement and have similar uncertainties. Therefore, we use the average of the three methods: $C = 0.34 \pm 0.02$.

III. MEASUREMENT OF OPTICAL THICKNESS AND TEMPERATURE

In this experiment we probe the atomic sample with a varying saturation parameter, up to relatively large values. The interaction with the light can thus have significant effects on the atomic cloud, in particular heating and pushing. It is therefore important to characterize the atomic sample taking into account those effects.

To this end, the optical depth of the cloud and its temperature are measured simultaneously to the data acquisition using interlaced cycles of subradiance measurements and absorption imaging as described in [7]. The same probe beam is used for both but absorption imaging is always performed at low saturation parameter and large detuning $\Delta = -4\Gamma$.

More precisely, absorption imaging was performed instead of the fluorescence measurement once every 250 cycles. Since during the data acquisition we are probing the atomic cloud with series of 12 laser pulses, to measure the optical thickness of the cloud corresponding to the nth pulse, we apply $(n-1)$ probe pulses before absorption imaging at the time corresponding to the nth pulse. This protocol enables us to have a good calibration of b_0 while probing our sample with laser pulses of different intensities.

The absorption imaging was also done for different times of flight, without and with a few applied probe pulses before, in order to measure the initial temperature of the cloud, as well as the heating induced by the pulses.

From those measurements we were able to extrapolate the temperature of the cloud after each of the 12 applied pulses. While the minimal temperature of the cloud that we measured is $T \approx 100\,\mu$K, the maximum temperature, considering the heating, is $T \approx 700\,\mu$K. As shown in [7], in this range of temperature, subradiance is not significantly affected: only a very slight decrease of the subradiant lifetime can be expected for the maximum considered temperature.

Another effect that could be relevant is the radiation-pressure force exerted by the probe beam on the cloud, inducing a velocity along the beam direction and correspondingly a Doppler shift, which changes the detuning seen by the atoms and thus the effective saturation parameter. This pushing effect can easily be computed and we have checked that, even for the highest saturation parameter, it only induces a very small reduction of the saturation parameter, which does not affect our results. This is confirmed by the fact that different values of b_0, corresponding to different times of flight and thus different numbers of applied pulses, yield similar results (see Fig.S4).

Finally, the expansion of the cloud during the pulse series is also responsible for a slight decrease of the ef-

fective intensity interacting with the cloud (due to the finite beam waist), of at most $\sim 20\%$. It does not affect significantly any of the presented results.

IV. SUBRADIANT DECAY CURVES

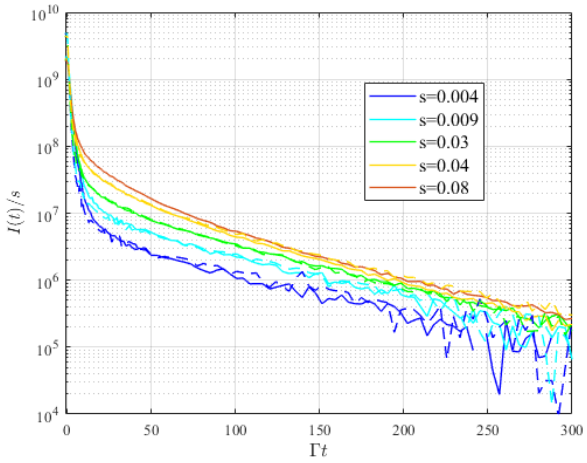

Fig. S 2. Temporal dynamics of the scattered intensity at the switch-off of the driving field, for different saturation parameters s as well as for $\Delta = -2\Gamma$ (solid line) and $\Delta = -4\Gamma$ (dashed line). The intensity curves are normalized by s. The amplitude of the slow decay increases with s and it is similar for both detunings.

In Fig. S2 we show typical experimental subradiant decay curves. This figure illustrates well the influence of the saturation parameter and detuning on the population of long-lived modes. Here, the scattered light intensity is normalized by the saturation parameter, and we only show values for $s \ll 1$. We observe that the amplitude of the slow decay, even after this normalization, increases with the saturation parameter, which illustrates well the superlinear behavior of the long-lived mode populations.

V. SUBRADIANT POPULATION USING EXACT SIMULATIONS

Simulations of the full Hilbert space are limited to small atom number. We here choose $N = 7$, with a cloud density $\rho_a = 0.03k^3$, to study the decay dynamics, performing an average of the intensity curves over 150 realizations. Following the same procedure as for other simulations to extract the population (i.e., through an exponential fit), we study its dependence on the saturation parameter. The scaling of the population P_- with the saturation parameter s is in good agreement with the one for the truncated simulations and the experimental: $P_- \propto s^{1.06\pm0.03}$ for the low-s regime and $P_- \propto s^{1.55\pm0.12}$ for the intermediate-s regime, see Fig.S3.

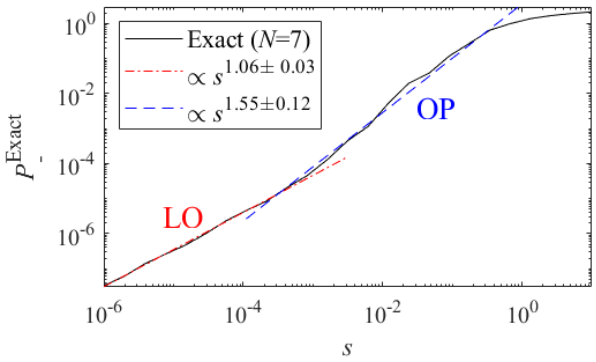

Fig. S 3. Population of the subradiant modes using exact simulations, with $N = 7$ atoms distributed randomly in a cloud of density $\rho_a = 0.03k^3$, and with a pump detuned by $\Delta = -2\Gamma$. The labels LO and OP stand, respectively, for the linear optics and optical pumping regime.

VI. SUPERLINEAR GROWTH WITH $s(\Delta)$ FOR SEVERAL b_0

In the main text the superlinear growth of the long-lived mode population as a function of the saturation parameter has been shown for an atomic sample of resonant optical thickness $b_0 = 54 \pm 2$ and two different detunings [Fig. 2(a)]. Here we demonstrate that this observation is robust by showing data acquired for different values of b_0. In Fig. S4 we show the normalized population P_- (see main text) as a function of s for $b_0 = 81 \pm 4$, $b_0 = 105 \pm 4$ and $b_0 = 163 \pm 5$. The obtained exponents of the power-law fit for $s < 0.04$ are $\beta \approx 1.47$, $\beta \approx 1.46$ and $\beta \approx 1.49$, respectively, demonstrating that the power-law scaling $\beta \sim 1.5$ is independent of b_0.

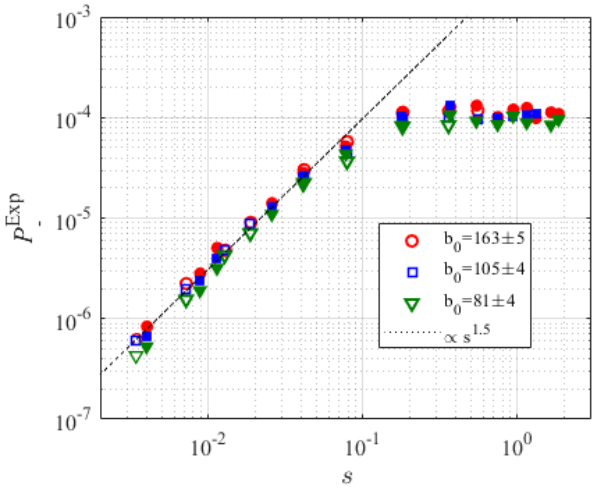

Fig. S 4. Normalized population P_- of long-lived modes as a function of the saturation parameter s for three different b_0, as well as $\Delta = -2\Gamma$ (filled circles) and $\Delta = -4\Gamma$ (empty circles). The results were obtained using the fit window $\Gamma t \in [150, 250]$.

VII. POPULATION OF MODES OF DIFFERENT LIFETIMES

Here we have investigated the behaviour of the subradiant modes with different lifetimes by monitoring the emission decay over different time windows: Later time analyses allow us to study longer-lived modes as they take longer to deplete. Over all the selected time windows, the super-linear scaling of the subradiant population P_- with the saturation parameter s is observed, see Fig. S5(a). The study of the associated lifetimes in Fig. S5(b) confirms that later-time dynamics is dominated by more subradiant modes. One can also observe that only the lifetimes extracted from the most-delayed fit window are independent of s because they correspond to single-excitation collective states. Indeed, increasing the pump strength leads to exploring subradiant states with shorter lifetimes, so the radiation from low-excitation subradiant states, with the largest lifetimes, may dominate only at later times.

Interestingly, in the regime where the populations grow super-linearly, they all have the same values (the curves of Fig. S5(a) collapse together). This suggests that the same population can be reached independently of the considered lifetimes. A first hint to understand the underlying mechanism can be found again in the case of $N = 2$ atoms: There, both the transitions $|ee\rangle \to |-\rangle$ and $|-\rangle \to |gg\rangle$ present a decay rate Γ_-. In a simple rate-equation approach, the population stored by optical pumping is expected to depend on the ratio between these rates, therefore the explicit dependence on Γ_- disappears.

From a numerical perspective, the low-b_0 clouds that can be simulated do not allow us to explore the behavior of modes with different lifetimes. As an alternative, we consider a system of $N = 5$ atoms in a small volume, organized as a regular chain for simplicity. Thus, the single-excitation collective modes are composed of one superradiant mode and four subradiant ones. Monitoring the steady-state population of these modes as a function of the saturation parameter reveals that, despite they exhibit very different levels in the "linear-optics regime" ($P_- \propto s$), the three most subradiant modes acquire the same populations in the regime where the modes are optically pumped [Fig. 5(c)]. Different chain lengths presented some fluctuations, but generally the populations have a strong tendency to reach the same values in that regime, suggesting that optical pumping induces an even population of the long-lived modes independently of their lifetimes.

The fact that the subradiant populations saturate, for large values of s, at different values in the experiment [Fig. S5(a)], is not observed in our small-system simulations [Fig. S5(c)]. It may thus be related to the large experimental cloud possessing a huge spectrum of subradiant modes, with a strong degeneracy of the energies (that is, a strong overlap between various modes), different from the latter test-system. Unfortunately, the simulations with the truncated system, limited to $b_0 \approx 5$, do not allow us to investigate the different lifetimes using larger systems ($N = 100$). One can only conclude that the huge Hilbert space at stake still holds many surprises.

[1] M. J. Stephen, The Journal of Chemical Physics **40**, 669 (1964).
[2] R. H. Lehmberg, Phys. Rev. A **2**, 883 (1970).
[3] R. Friedberg, S. R. Hartmann, and J. T. Manassah, Phys. Rep. C **7**, 101 (1973).
[4] M. Gross and S. Haroche, Physics Reports **93**, 301 (1982).
[5] J. Cremer, D. Plankensteiner, M. Moreno-Cardoner, L. Ostermann, and H. Ritsch, "Polarization control of radiation and energy flow in dipole-coupled nanorings," (2020), arXiv:2004.09861.
[6] A. Cipris, R. Bachelard, R. Kaiser, and W. Guerin, "Van der waals dephasing for dicke subradiance in cold atomic clouds," (2020), arXiv:2012.06248.
[7] P. Weiss, A. Cipris, M. O. Araújo, R. Kaiser, and W. Guerin, Phys. Rev. A **100**, 033833 (2019).

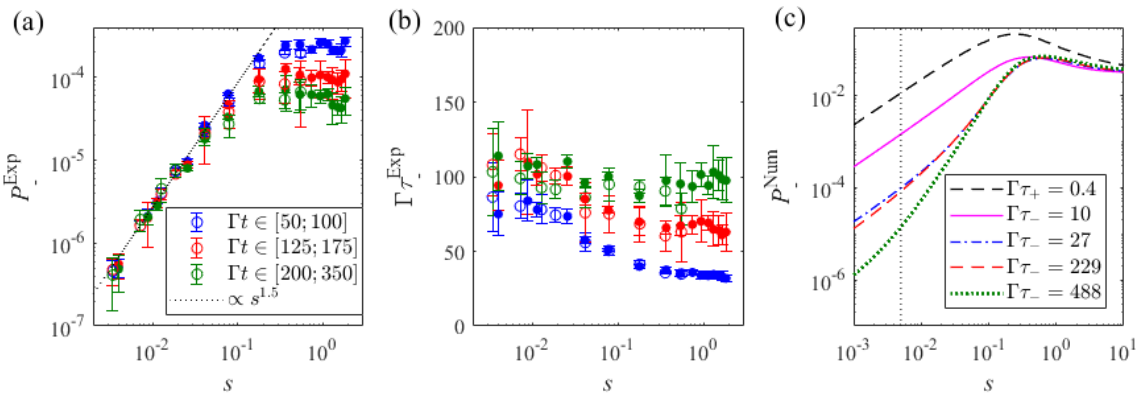

Fig. S 5. (a) Subradiant population P_- (b) and associated lifetimes $\Gamma\tau_-$ as a function of the saturation parameter, obtained from the fit over different time windows. The optical depth is $b_0 \approx 80$. Filled and empty symbols are for $\Delta = -2\Gamma$ and $\Delta = -4\Gamma$, respectively. (c) Population of the single-excitation collective modes for a linear regular chain of length $kL = 1$, with a pump in the direction of the chain and a detuning $\Delta = -200\Gamma$. The vertical black dotted line marks the saturation value around which the population of the most subradiant modes departs from the linear-optics behaviour.